Kinetics and Catalysis, Vol. 43, No. 3, 2002, pp. 433–442. From Kinetika i Kataliz, Vol. 43, No. 3, 2002, pp. 468–478.

Stability and Deactivation of Au/Fe_2O_3 Catalysts for CO Oxidation at Ambient Temperature and Moisture*

Gui Ying Wang, Hong Lei Lian, Wen Xiang Zhang, Da Zhen Jiang, and Tong Hao Wu

Department of Chemistry, Jilin University, Changchun, 130023, P. R. China

Received April 24, 2001

Abstract—Various Au/Fe_2O_3 catalysts were prepared by the coprecipitation method, and CO oxidation was studied at ambient temperature and in the presence of water vapor in the feed. It was found that the precipitation method and the calcination temperatures have a significant effect on the catalytic performance of CO oxidation. The stability is related to the particle size of metallic gold and α-Fe_2O_3 and the oxidation state of gold and the iron crystalline phase. The sintering of the gold particles, the reduction of oxide gold to metallic gold, the accumulation of carbonate, and a decrease in the specific surface area were observed during the reaction, which may contribute to the deactivation of Au/Fe_2O_3 catalysts.

INTRODUCTION

Low-temperature carbon monoxide oxidation is a very significant way to purify air in closed spaces and offices, to reduce CO in industrial and automobile emissions, and to detect CO [1–3]. In many cases, air purification and CO detection involve CO oxidation at a low concentration in air containing substantial amounts of water. For practical application, catalysts should exhibit high activity for long periods at room temperature and in the presence of water vapor. Hopcalite catalysts (mainly composed of MnO_x and CuO) are the most important commercial catalysts for CO oxidation. However, they are unstable in the presence of water and have low activity at room temperature [3]. Supported Pt, Pd, Ru, and Rh catalysts exhibit appreciable activity for CO oxidation only at temperatures higher than 150°C [4]. A search for new catalysts for CO oxidation at ambient temperature is, therefore, an important task. Haruta and co-workers have shown that Au supported on metal oxides can provide catalysts with high activity even at temperatures below 0°C [3–6]. These surprising results attracted much attention and subsequent studies confirmed the high activity of Au-containing catalysts for low-temperature CO oxidation [7–28]. However, most of the catalysts are only efficient over a short period of time, especially in the presence of water in the feed mixture, and some gold catalysts such as Au/MnO_x [7, 8, 25], Au/TiO_2 [9, 10], and Au/ZrO_2 [11] rapidly deactivate. Therefore, the catalysts with improved stability and water-resistance are strongly required.

Although Au/Fe_2O_3, Au/Co_3O_4, Au/NiO, and Au/TiO_2 [4, 5, 10–17] catalysts have been relatively well studied, there have been few detailed studies on the stability and deactivation mechanism of Au-based catalysts. In this paper, the catalytic stability of Au/Fe_2O_3 catalysts for room-temperature CO oxidation was investigated in detail, and we paid more attention to the effects of the precipitation method and calcination temperatures. The Au/Fe_2O_3 catalysts before and after CO oxidation were characterized by XRD, TEM, BET, TPR, XPS, Mössbauer and *in situ* FTIR spectroscopy, and possible explanations for deactivation are given.

EXPERIMENTAL

$HAuCl_4 \cdot 4H_2O$ (99.9%), $Fe(NO_3)_3 \cdot 9H_2O$ (99%), and Na_2CO_3 (99%) were used as starting materials for the preparation of Au/Fe_2O_3 catalysts. Four different preparation procedures were used.

Method A: An aqueous solution of $Fe(NO_3)_3$ and $HAuCl_4$ (Au : Fe = 1 : 50, atomic ratio, 84.144 mmol in 150 ml H_2O) was added dropwise (2 ml/min) to an aqueous solutions of Na_2CO_3 (127.05 mmol in 120 ml H_2O) under conditions of vigorous stirring. The final pH achieved varied between 7.0 and 8.2. After 4 h of aging at room temperature, the precipitate was filtered and washed with hot deionized water (~50°C) several times until no Cl^- was detected by $AgNO_3$ solution in the filtrate. The product was dried in air at 50°C for 24 h, before the test sample was calcined at 300°C for 4 h in a flow of 20% O_2/Ar. The catalyst thus obtained is denoted as Au/Fe_2O_3/A.

Method B: Na_2CO_3 (127.05 mmol in 120 ml H_2O) aqueous solution was added dropwise (2 ml/min) into an aqueous mixture of $Fe(NO_3)_3$ and $HAuCl_4$ (Au : Fe = 1 : 50, atomic ratio, 84.144 mmol in 150 ml H_2O), and the rest of the procedure was similar to method A. The catalyst is denoted as Au/Fe_2O_3/B.

Method C: Aqueous solutions of $Fe(NO_3)_3$ (82.494 mmol in 130 ml H_2O) were first added drop-

* This article was submitted by the authors in English.

0023-1584/02/4303-0433$27.00

wise (2 ml/min) to Na_2CO_3 (127.05 mmol in 120 ml H_2O) solution; then, $HAuCl_4$ (1.650 mmol in 20 ml H_2O) solution was added dropwise (2 ml/min) under conditions of vigorous stirring, and the rest of the procedure was similar to method A. The catalyst is denoted as $Au/Fe_2O_3/C$.

Method D: An aqueous mixture of $Fe(NO_3)_3$ and $HAuCl_4$ (Au : Fe = 1 : 50 atomic ratio, 84.144 mmol in 150 ml H_2O) was poured into an aqueous solution of Na_2CO_3 (127.05 mmol in 120 ml H_2O) under conditions of vigorous stirring, and the rest of the procedure process was similar to method A. The catalyst is denoted as $Au/Fe_2O_3/D$.

To investigate the effect of the calcination temperatures on the properties of Au/Fe_2O_3 catalysts, the dried Au/Fe_2O_3 catalyst prepared by method A was split into five portions and calcined at different temperatures: 100, 200, 300, 400, and 500°C. These samples are denoted as Au/Fe_2O_3-*T*, where *T* is the calcination temperature, °C. Fe_2O_3 was prepared by method A and calcined at 300°C.

X-ray powder diffraction (XRD) patterns were recorded on a D/Max-rA X-ray diffractometer operated at 50 kV and 150 mA using nickel-filtered CuK_α radiation and at a scanning rate of 0.2° (2θ)/s in the range 20°–70°, and at a scanning rate of 0.002° (2θ)/s in the range 37°–39° to detect metallic Au crystalline phase clearly. The mean crystalline size was estimated from the full width at the half-maximum (FWHM) of the X-ray diffraction peak using the Scherrer equation with a correction for instrument line broadening.

Transmission electron microscopic (TEM) images were obtained using an H8100-IV electron microscope operated at 200 kV. At least 100 particles were used to determine the mean diameter of the Au particles.

The surface areas of the samples were measured by a conventional BET nitrogen adsorption method (N_2 99.999%) at –196°C using an ASAP 2010 instrument. Before measurements, samples (~0.3 g) were treated at 300°C (or at the calcination temperatures) for 2 h in a vacuum.

X-ray photoelectron spectroscopy (XPS) measurements were conducted on a VG ESCALAB MK II spectrophotometer using MgK_α radiation for X-ray excitation under pressures lower than 5×10^{-7} Pa. The electron binding energies were referenced to the C1*s* (E_b = 284.6 eV) peak.

TPR measurement was conducted in a homebuilt flow system. Catalyst samples of 20 mg were placed in a quartz cell, pretreated in Ar at 50°C for 30 min, and an H_2 :Ar (5 : 95 vol) gaseous mixture was introduced into the cell. Water produced by reduction was trapped in a 5 Å molecular sieve column. The temperature of the samples was raised at a constant rate of 10°C/min, and H_2 uptake during reduction was measured using a Shimadzu GC-8A gas chromatograph (TCD).

The ^{57}Fe Mössbauer experiments were carried out on an MS-500 constant acceleration spectrometer equipped with a ^{57}Co source. The velocity scale was adjusted according to α-Fe at 25°C. The spectra were fitted with appropriate superpositions of Lorentz lines. In this way, spectral parameters, such as the isomer shift, the electron quadrupole splitting, the full linewidth at half maximum, the magnetic hyperfine field, and the relative resonance areas of different components of the absorption patterns were determined.

FT-IR spectra were measured on a Nicolet Impact 410 spectrometer at a spectral resolution of 2 cm^{-1}. Sample powders were pressed into self-supported thin disks with a diameter of 2 cm and placed in an IR quartz cell allowing thermal treatment in a vacuum or in a controlled atmosphere. First, the sample was calcined at 300°C in air for 3 h, evacuated for 2 h at the same temperature and pressures less than 5×10^{-6} Pa, and then cooled to 25°C. Carbon monoxide and oxygen (26.7 kPa CO and 26.7 kPa O_2) were admitted into the IR cell, and the IR spectra were recorded at different reaction times.

The catalytic activity of the Au/Fe_2O_3 catalysts for carbon monoxide oxidation was carried out in a continuous flow fixed-bed reactor (0.6 cm i.d.) under atmospheric pressure at 25°C. The catalyst sample (0.50 g) was loaded in each run, and the O_2–CO–Ar mixture bubbled through a water vapor saturator at a flow rate of 100 ml/min. The gas mixture consisted of 0.5% CO, 10% O_2, 1.8% H_2O, and balance Ar. The reaction products were analyzed by on-line gas chromatography using a column of GDX-502 for CO_2 and a 5 A molecular sieve column for CO and O_2. The catalytic activity was expressed as a degree of CO conversion. The lifetime of the catalyst was defined as the reaction time during which the CO conversion remains higher than 99%.

RESULTS AND DISCUSSION

Effect of the Precipitation Method

Figure 1 shows the conversion of CO to CO_2 over Au/Fe_2O_3 catalysts prepared by various methods as a function of time-on-stream. It is seen that the complete conversion of CO can be obtained over the four samples. The activity is stable for a certain period and then decreases with reaction time. The lifetimes of the Au/Fe_2O_3 catalysts are obviously different, the stability series is $Au/Fe_2O_3/A > Au/Fe_2O_3/B > Au/Fe_2O_3/C > Au/Fe_2O_3/D$. Method A is the best for preparing Au/Fe_2O_3 catalysts that can completely transform CO into CO_2 for more than 380 h.

The XRD patterns of Au/Fe_2O_3 catalysts prepared by different methods are shown in Fig. 2. All catalysts exhibit the α-Fe_2O_3 phase [32]. However, subtle differences are apparent. For the $Au/Fe_2O_3/A$ catalysts, the XRD peaks at 2θ = 38.2° and 2θ = 44.4° for metallic gold crystallites are barely observed. For the Au/Fe_2O_3 catalysts prepared by methods B, C, and D, the intensity and sharpness of metallic Au peaks gradually

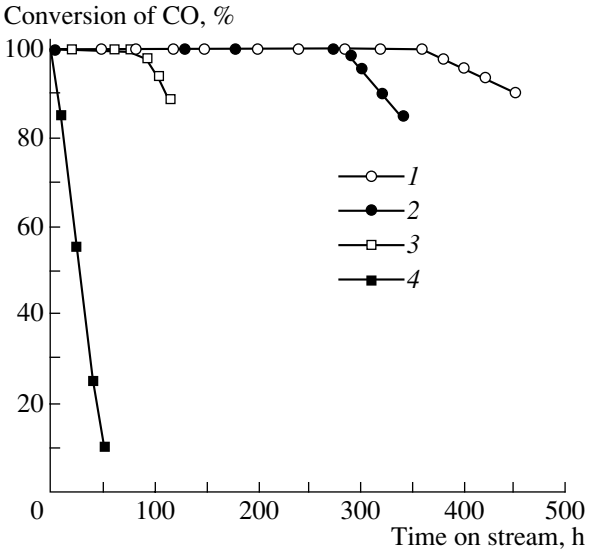

Fig. 1. Effect of the precipitation method on CO oxidation over the Au/Fe_2O_3 catalysts calcined at 300°C: (*1*) Au/Fe_2O_3/A, (*2*) Au/Fe_2O_3/B, (*3*) Au/Fe_2O_3/C, (*4*) Au/Fe_2O_3/D. Reaction conditions: 25°C, 0.5% CO, 10% O_2, 1.8% H_2O, total flow rate of 100 ml/min.

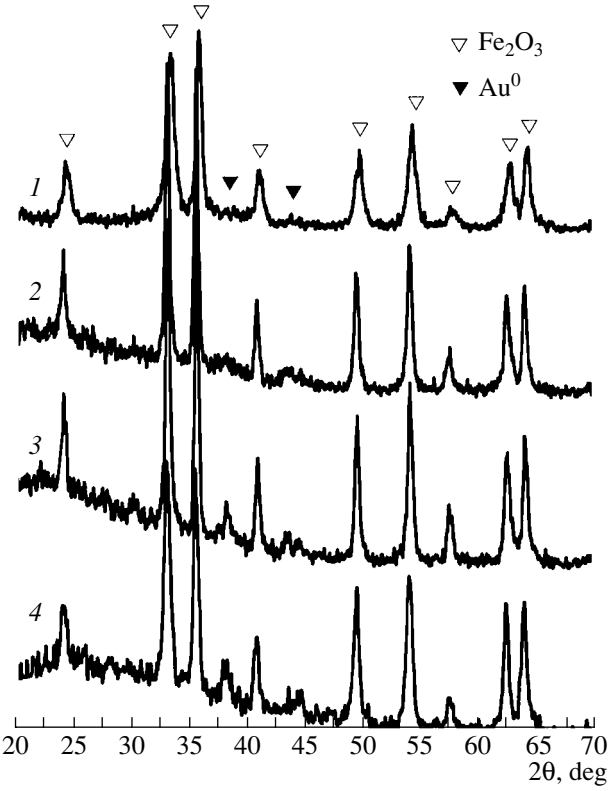

Fig. 2. X-ray diffraction patterns for Au/Fe_2O_3 catalysts prepared by different precipitation methods calcined at 300°C. (*1*) Method A, (2) method B, (*3*) method C, and (*4*) method D. Reaction conditions: 25°C, 0.5% CO, 10% O_2, 1.8% H_2O, total flow rate of 100 ml/min.

increase, the mean diameters of metallic Au calculated by the Scherrer equation are 4.0, 5.4, and 6.3 nm, respectively.

Figures 3a and 3b show the TEM image and the size histograms of gold particles of the Au/Fe_2O_3/A catalyst. Deposited gold particles that appear as small black spots are uniformly dispersed on the surface of α-Fe_2O_3, and the diameter of gold particles is in the range 1.6–6 nm with a mean diameter of ca. 3.4 nm.

From the above results, it can be found that the Au particle size is strongly dependent on the preparation procedure, following the series Au/Fe_2O_3/A < Au/Fe_2O_3/B < Au/Fe_2O_3/C < Au/Fe_2O_3/D, which is opposite to the order of the lifetimes. Therefore, the stability of Au/Fe_2O_3 catalysts is probably related to the particle size of gold, and the small Au particle size is beneficial for enhancing the lifetime of the Au/Fe_2O_3 catalysts.

Effect of the Calcination Temperatures

The initial CO conversion and the lifetime of Au/Fe_2O_3-*T* (*T* = 100–500) are summarized in Table 1. All Au/Fe_2O_3 samples calcined at 100–500°C provide the complete oxidation of CO to CO_2 under our experimental conditions. If the catalysts are calcined at 100–300°C, the lifetime ranges from 348 to 380 h, which is a short range. For the calculation temperatures above 400°C, the lifetime significantly shortens, and the effective calculation temperature ranges from 100 to 300°C.

Figures 4a and 4b shows the XRD patterns of Au/Fe_2O_3-*T* (*T* = 100–500) catalysts before (fresh) and after (used) CO oxidation. Figure 4a shows that fresh catalysts calcined at <200°C show similar diffraction patterns which mainly correspond to amorphous ferrihydrite [29–32] or comprise the poorly crystalline phases of ferrihydrite and α-Fe_2O_3 (hematite) [32]. After calcination at > 300°C, the α-Fe_2O_3 phase can be observed in the samples and the intensity of α-Fe_2O_3 XRD peaks gradually increases with an increase in the calcination temperatures. The corresponding half-widths of peaks became narrower. These facts indicate that the amorphous ferrihydrite can decompose into Au/Fe_2O, and Au/Fe_2O_3-*T* particles agglomerate during the calcination process; accordingly, the specific surface area of the samples also decreases (Table 1).

It can also be found from Figs. 4a, 4b that no XRD peaks of metallic Au (2θ = 38.2°, 44.4°) and/or Au_2O_3 (2θ = 25.5°, 30.2°, and 32.5°) [32] species are detected in the Au/Fe_2O_3-*T* (*T* ≤ 300). This implies that gold particles are highly dispersed on the surface of amorphous ferrihydrite and/or crystalline α-Fe_2O_3, or the amount of gold species is smaller than that of the detectable content by XRD technique. Because gold particles will sinter with an increase in the calcination temperatures [3, 9], the mean diameter of gold particles in Au/Fe_2O_3-*T* (*T* = 100–200) catalysts may be smaller than in the Au/Fe_2O_3-300 catalysts with a mean diameter of

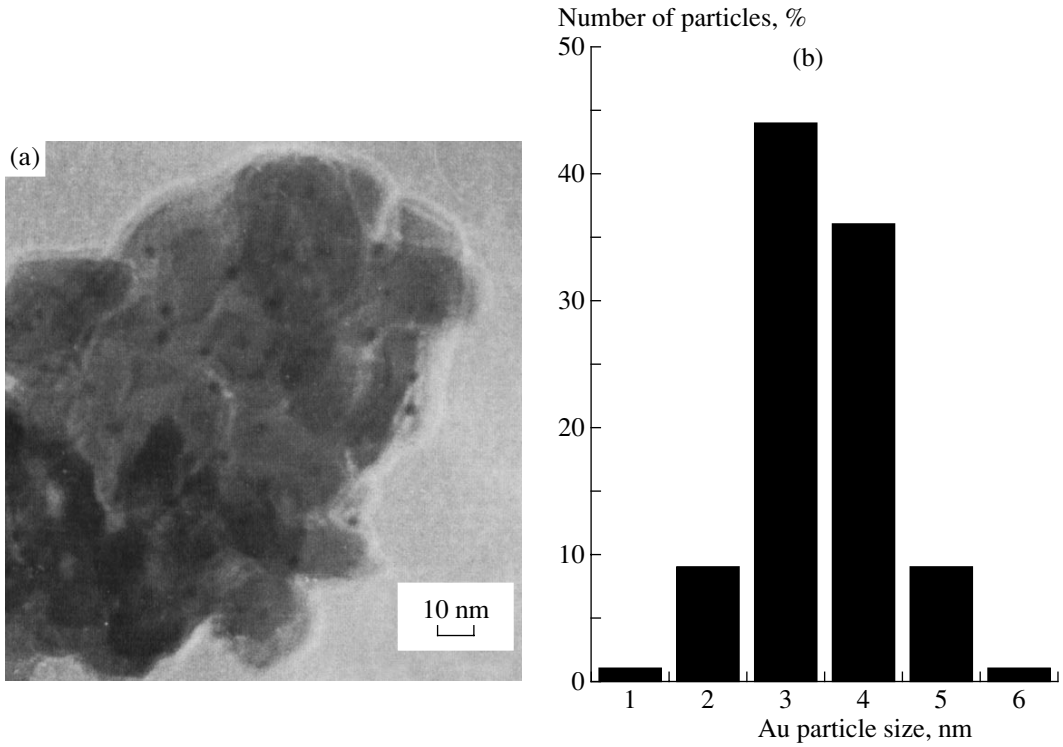

Fig. 3. TEM photograph of fresh Au/Fe_2O_3 catalysts prepared by method A and calcined at 300°C (a) and Au particles distribution diagram (b). Mean d_{Au} = 3.4 nm.

3.4 nm. When the catalysts were calcined above 400°C, the XRD peaks of metallic gold appear and become more intense and sharper with an increase in the calcination temperature. The mean diameter of metallic Au particles in Au/Fe_2O_3-400 and Au/Fe_2O_3-500 calculated by the Scherrer equation is about 5.0 and 6.0 nm, respectively. Taking into account this observation, we conclude that the metallic Au particles agglomerate during the calcination process and become more important at higher temperatures.

Figures 5a, 5b show the XPS spectra of fresh Au/Fe_2O_3 catalysts calcined at 100–400°C. As shown in Fig. 5a, the Fe*2p* pattern for the Au/Fe_2O_3 catalysts calcined at different temperatures exhibit a large peak at an E_b value of 711.4 eV and a satellite peak at a higher E_b value of 715–725 eV, which can be assigned to Fe(III) species.

Figure 5b compares the XPS of Au4$f_{1/2}$ for fresh Au/Fe_2O_3-*T* (*T* = 100–400) catalysts. The fresh Au/Fe_2O_3-100 shows peaks at BE values of 86.5 for Au4$f_{1/2}$ and 90.1 eV for Au4$f_{5/2}$ lines, respectively. These binding energies are close to the Au4*f* binding energies of Au_2O_3 [12, 30]. After calcination at 200°C, three broad peaks appear near the Au4*f* binding energies of Au_2O_3 and metallic Au indicating that oxide and metallic Au coexist in the samples. When calcined at

Table 1. The initial CO conversion, lifetime, specific surface area, and mean diameter of Au over Au/Fe_2O_3-*T* (*T* = 100–500°C) catalysts

Catalysts	Initial CO conversion	Lifetime (h)	S_{BET}, m^2/g		Mean d_{Au}, nm	
			fresh	used	fresh	used
Au/Fe_2O_3-100	100	348	178.5	143.1	<3.4*	6.9*
Au/Fe_2O_3-200	100	370	121.5	130.4	<3.4*	8.0*
Au/Fe_2O_3-300	100	380	78.4	75.7	3.4**	9.7*
Au/Fe_2O_3-400	100	260	38.6	36.3	5.0*	10.3*
Au/Fe_2O_3-500	100	40	21.7	20.9	6.0*	9.8*

Note: Reaction conditions: 25°C, 0.5% CO, 10% O_2, 1.8% H_2O, GHSV = 12000 h^{-1}. Fresh/used: before/after CO oxidation.

* XRD results.

** TEM results.

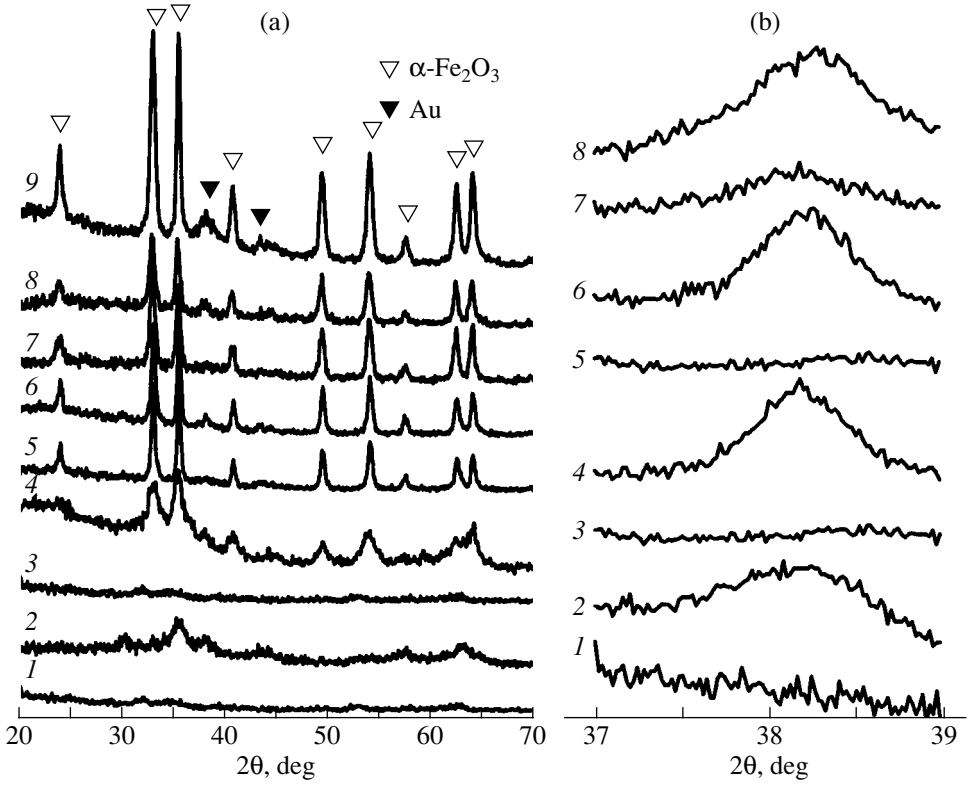

Fig. 4. X-ray diffraction patterns for Au/Fe_2O_3 catalysts calcined at different temperature. (a) (*1*) 100°C fresh, (*2*) 100°C used, (*3*) 200°C fresh, (*4*) 200°C used, (*5*) 300°C fresh, (*6*) 300°C used, (*7*) 400°C fresh, (*8*) 400°C used, and (*9*) 500 fresh. (b) (*1*) 100°C fresh, (*2*) 100°C used, (*3*) 200°C fresh, (*4*) 200°C used, (*5*) 300°C fresh, (*6*) 300°C used, (*7*) 400°C fresh, and (*8*) 400°C used. Reaction conditions: 25°C, 0.5% CO, 10% O_2, 1.8% H_2O, total flow rate of 100 ml/min.

400°C, only two distinct peaks appear at 83.7 and 87.4 eV, which are close to the Au4*f* binding energies of metallic Au [12, 30]. To quantitatively determine the relative portion of Au_2O_3 and metallic gold, the deconvolution of Au4*f* peaks was performed, and the results are listed in Table 2. The gold phase is transformed progressively from oxide to metallic gold as the calcination temperatures increases, and the pure metallic Au phase is formed after calcination above 400°C.

Figure 6 shows the TPR spectra of α-Fe_2O_3 calcined at 300°C and Au/Fe_2O_3-*T* (*T* = 100, 200, 300, 400, and 500) before and after CO oxidation. The TPR spectrum of α-Fe_2O_3 contains two peaks, one of which with T_{max} at about 390°C is related to the $Fe_2O_3 \longrightarrow Fe_3O_4$ reduction step, whereas the other at about 660°C is attributed to the transition $Fe_3O_4 \longrightarrow FeO \longrightarrow Fe$ [33]. Fresh Au/Fe_2O_3-*T* (*T* = 100, 200, and 300) catalysts mainly show three peaks denoted as I, II, and III from low to high temperature, respectively. The peak I area decreases with an increase in the calcination temperature. After calcination above 400°C, peak I disappears and only peaks II and III can be observed. TPR and XPS data suggest that peak I may be related to the reduction of Au oxide. At higher calcination temperatures, the amount of Au oxide in fresh Au/Fe_2O_3-*T* catalysts gradually reduces. On the other hand, the TPR spectra of Au/Fe_2O_3-300 substantially differ from those of α-Fe_2O_3: peaks II and III in the fresh Au/Fe_2O_3-300 catalyst markedly shifted toward a lower temperature compared to the α-Fe_2O_3 samples. This means that Au species (oxide or/and metal) strongly influence the reducibility of iron species. This is probably due to the polarization of the Fe–O bonds by $Au^{\delta+}$ (δ = 0–3), or there may exist synergistic interaction between Au and Fe_2O_3 [4, 5, 13, 14], which result in the easier reduction of Fe_2O_3 species in Au/Fe_2O_3 catalysts. Furthermore, Au species (oxide or metallic) in the Au/Fe_2O_3 catalysts could activate H_2 [3]. Then, the activated H species spillover to the interface of gold, and iron promotes the reduction of the Fe oxide species.

Figure 7 shows the room temperature ^{57}Fe Mössbauer spectra of Au/Fe_2O_3-*T* (*T* = 100, 200, 300, and 400) catalysts before and after CO oxidation tests. The results of the least-squares fit of all spectra are compiled in Table 3. Three main features are observed. The first typical component is a broadened electric quadrupole doublet with an isomer shift of about 0.35 mm/s and a splitting of about 0.75 mm/s. These parameters are typical for ferrihydrite [13, 28–31], while they also might be attributed to superparamagnetic hematite, i.e.,

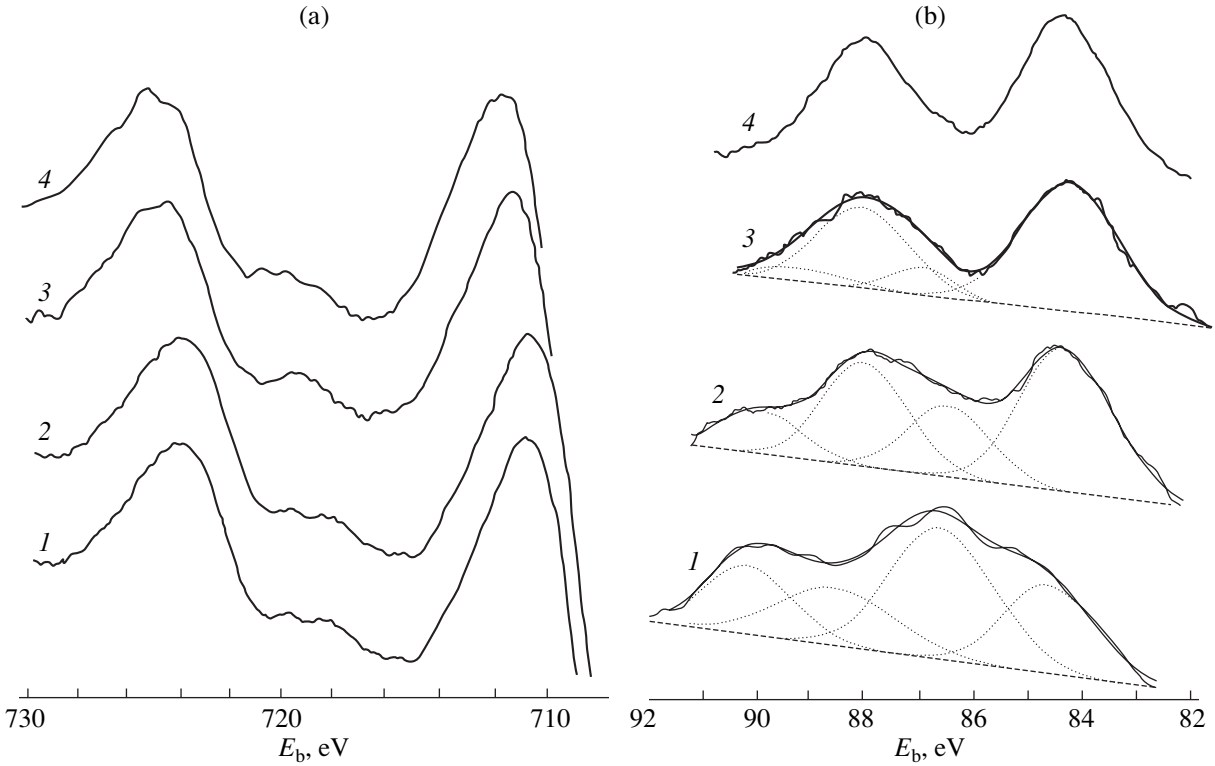

Fig. 5. XPS spectra of Fe 2*p* (a) and Au4*f* region (b) for fresh Au/Fe_2O_3 catalysts calcined at different temperature. (a) (*1*) 100°C fresh, (*2*) 200°C fresh, (*3*) 300°C fresh, and (*4*) 400°C fresh. (b) (*1*) 100°C fresh, (*2*) 200°C fresh, (*3*) 300°C fresh, and (*4*) 400°C fresh.

to the hematite particles smaller than ~8 nm [13, 29–31]. Since hematite particles small enough to be superparamagnetic at ambient temperature are rarely formed in concentrated iron systems, the doublet spectrum was attributed to ferrihydrite. The second feature is a sextuplet with a magnetic hyperfine field of 465 KOe or more, which can unambiguously be attributed to hematite [13, 29–31]. The third feature is also a sextuplet with a magnetic hyperfine field of 440–450 KOe, which can be assigned to the large ferrihydrite particles [30]. Table 3 shows the relative spectra areas of ferrihydrite and hematite components in the Mössbauer spectra of Au/Fe_2O_3 catalysts calcined at different temperatures. With these assignments, several conclusions can be drawn: the fresh Au/Fe_2O_3-100 catalysts mainly consist of ferrihydrite. With an increase in the calcination temperatures, the relative portion of ferrihydrite gradually decreased, whereas the amount of hematite increased. When the sample is calcined at 400°C, ferrihydrite completely vanish. These results demonstrate further that ferrihydrite gradually transforms into α-Fe_2O_3 with an increase in the calcination temperature. It is worth noting that, although no obvious Au/Fe_2O_3-200 crystalline diffraction peaks were observed in the XRD spectrum for the fresh Au/Fe_2O_3-200 catalysts, there are two sextuplets assigned to α-Fe_2O_3 (H = 479–483 kOe) and the larger particles of ferrihydrite (H = 440–448 kOe) [30] in the Mössbaur spectrum. This suggests that α-Fe_2O_3 is highly dispersed as relatively small crystallites and/or as poor crystallites in fresh Au/Fe_2O_3-200 catalysts, so it was not detected by X-ray diffraction.

Table 2. Au4$f_{7/2}$ binding energy, FWHM, and relative proportions of the various gold species in Au/Fe_2O_3-*T* (*T* = 100–400) catalysts

Catalysts	*E* (Au4$f_{7/2}$), eV		*W*, eV		Au species, %	
	I	II	I	II	I	II
Au/Fe_2O_3-100	86.5	86.4	1.3	1.2	Au_2O_3 (63)	Au_2O_3 (25)
Au/Fe_2O_3-200	86.3	86.1	1.8	1.8	Au_2O_3 (30)	Au_2O_3 (8)
Au/Fe_2O_3-300	83.9	83.7	2.1	2.0	Metallic Au (88)	Metallic Au (100)
Au/Fe_2O_3-400	83.7	83.6	2.0	1.9	Metallic Au (100)	Metallic Au (100)

Note: I—fresh and II—used catalysts. Reaction conditions: 25°C, 0.5% CO, 10% O_2, 1.8% H_2O.

It can be inferred from the lifetimes and characteristics of the Au/Fe_2O_3 catalysts calcined at different temperatures that Au/Fe_2O_3 catalysts calcined at temperatures above 300°C have a similar α-Fe_2O_3 phase, although a decrease in the lifetime with an increase in the calcination temperature could be due to the sintering of gold and the agglomeration of α-Fe_2O_3. These results demonstrate once again that the stability is related to the particle size of gold and α-Fe_2O_3.

For Au/Fe_2O_3 catalysts calcined at temperatures below 300°C, the physical and chemical properties of iron and gold in catalysts such as concentration, crystallinity, SBET, particle size, and other characteristics changed with the calcination temperature. Hence, the influence of these factors on the stability of Au/Fe_2O_3 catalysts is very complex. In these catalysts, the mean diameter of gold particles does not vary a lot, while the retained amount of Au oxide is obviously different (Table 2). Clearly, both metallic gold and oxidized gold species are responsible for the catalytic oxidation of CO in addition to the particle size in this case. However, quantitative correlation between the relative amount of gold species present on the catalyst and the lifetime is not clear, and detailed studies are in progress. On the other hand, when gold exists in the form of nanoparticles dispersed on the surface of the catalysts, both ferrihydrite and hematite in the Au/Fe_2O_3 catalysts also have a significant effect on the catalytic performances of CO oxidation.

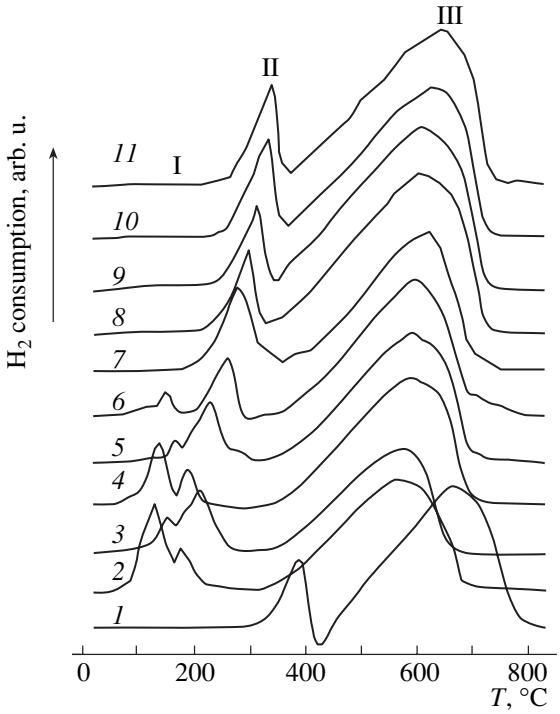

Fig. 6. TPR spectra of Fe_2O_3 and Au/Fe_2O_3 catalysts calcined at different temperature, (*1*) Fe_2O_3, (*2*) 100°C fresh, (*3*) 100°C used, (*4*) 200°C fresh, (*5*) 200°C used, (*6*) 300°C fresh, (*7*) 300°C used, (*8*) 400°C fresh, (*9*) 400°C used, (*10*) 500 fresh. Reaction conditions: 25°C, 0.5% CO, 10% O_2, 1.8% H_2O, GHSV = 12000 h^{-1}.

Investigation of Deactivation Mechanism for Au/Fe_2O_3 Catalysts

As follows from Fig. 1 and Table 1, all the Au/Fe_2O_3 catalysts deactivate during reaction. The decay rate is strongly dependent on the precipitation method and calcination temperatures. In order to explore the deactivation reason of Au/Fe_2O_3 catalysts, the fresh and used Au/Fe_2O_3 catalysts were characterized by XRD, Mössbauer, BET, XPS, TPR and *in situ* FTIR.

Table 3. ^{57}Fe Mössbauer parameters for Au/Fe_2O_3-*T* (*T* = 100–400°C) catalysts at 25°C

Sample	Multiplet		IS, mm/s		QS, mm/s		*H*, kOe		$W_{1/2}$, mm/s		*Y*, %		Assignment	
	I	II	I	II	I	II	I	II	I	II	I	II	I	II
Au/Fe_2O_3-100	Doublet	Doublet	0.35	0.32	0.75	0.74	–	–	0.25	0.28	100	40	Ferrihydrite	Ferrihydrite
		Sextuplet 1		0.30		0.06		469.71		1.42		60		Hematite
Au/Fe_2O_3-200	Doublet	Doublet	0.33	0.32	0.79	0.77	–	–	0.31	0.31	32	26	Ferrihydrite	Ferrihydrite
	Sextuplet 1	Sextuplet 1	0.34	0.37	0.24	0.21	479.68	483.37	0.26	0.21	15	24	Hematite	Hematite
	Sextuplet 2	Sextuplet 2	0.32	0.32	–0.06	0.11	439.54	444.49	1.37	1.05	53	50	Ferrihydrite*	Ferrihydrite*
Au/Fe_2O_3-300	Doublet	Doublet	0.33	0.31	0.80	0.78	–	–	0.29	0.30	8	5	Ferrihydrite	Ferrihydrite
	Sextuplet 1	Sextuplet 1	0.35	0.35	0.23	0.20	505.90	507.56	0.15	0.16	40	37	Hematite	Hematite
	Sextuplet 2	Sextuplet 2	0.36	0.36	0.23	0.20	483.95	481.27	0.52	0.40	52	58	Hematite	Hematite
Au/Fe_2O_3-400	Sextuplet 1	Sextuplet 1	0.35	0.35	0.21	0.21	512.07	510.75	0.17	0.17	100	100	Hematite	Hematite

Notes: I—fresh and II—used catalysts. Reaction conditions: 25°C, 0.5% CO, 10% O_2, 1.8% H_2O, GHSV = 12000 h^{-1}. IS, isomer shift; QS, quadrupole splitting; *H*, hyperfme field; $W_{1/2}$, half width at half maximum; *Y*, area ratio.

* Large ferrihydrite.

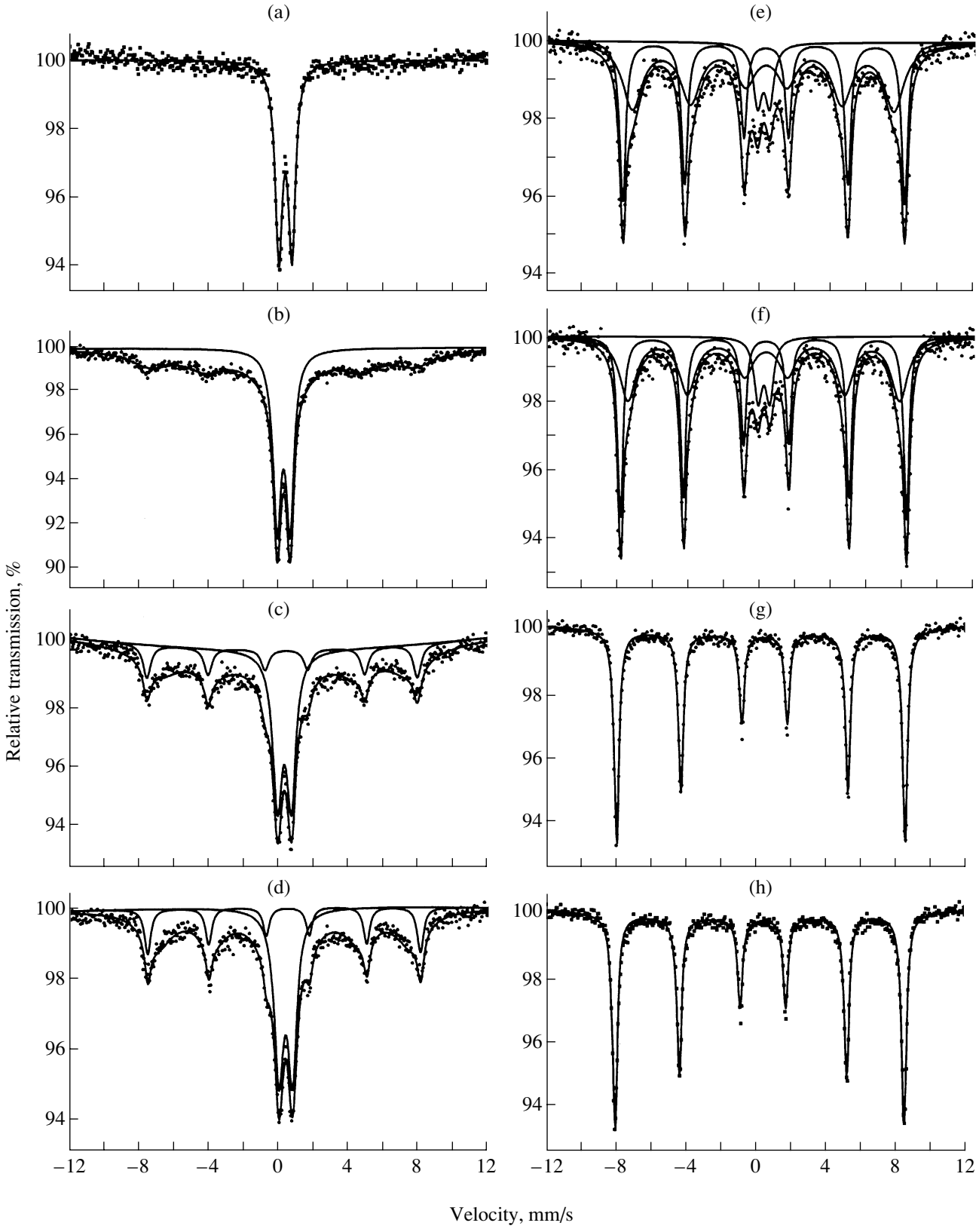

Fig. 7. ^{57}Fe Mössbauer spectra for Au/Fe_2O_3 catalysts calcined at different temperature before and after CO oxidation: (a) 100°C fresh, (b) 100°C used, (c) 200°C fresh, (d) 200°C used, (e) 300°C fresh, (f) 300°C used, (g) 400°C fresh, (h) 400°C used. Reaction conditions: 25°C, 0.5% CO, 10% O_2, 1.8% H_2O, total flow rate of 100 ml/min.

The XRD patterns of the used Au/Fe_2O_3-*T* (*T* = 100, 200, 300, 400) catalysts are shown in Figs. 4a, 4b. The differences in the XRD patterns are observed between the used catalysts and their fresh analogues. First, the metallic gold reflections Au(111) (2θ =38.2°) appear in the used Au/Fe_2O_3-*T* (*T* = 100–300) catalysts, and the gold peaks of Au/Fe_2O_3-400 are significantly stronger and sharper than those of the fresh samples. These results indicate that metallic gold might agglomerate during CO oxidation at room temperature and moisture (Table 1). Because the size of gold particles is one of the crucial factors that influences the activity of the gold-based catalysts, the activity is inversely proportional to the square diameter of gold particles [3, 10]. Because the gold particle size gradually increases with reaction time, the activity of Au/Fe_2O_3 catalysts reduces.

Second, as shown in Fig. 4a, some new XRD peaks (2θ = 24.2°, 33.2°, 35.7°, 40.9°, 49.5°, 54.2°, 62.5°, and 64.0°) appear in the used Au/Fe_2O_3-100 and Au/Fe_2O_3-200 samples, which could be assigned to α-Fe_2O_3. This suggests that the amorphous ferrihydrite species transform into α-Fe_2O_3 crystalline during reaction, which is also confirmed by Mössbauer data of Au/Fe_2O_3-*T* (*T* = 100–300) (Table 3 and Fig. 7). Wanger *et al.* [13, 30, 31] reported that the ferrihydrite in the Au/Fe_2O_3-100 catalyst is important for the activation of molecular oxygen, and the activity in CO oxidation could be enhanced by an increase in the relative amount of ferrihydrite increased. Therefore, the ferrihydrite transformed into α-Fe_2O_3 may be contributed to the decay of activity to some extent.

As follows from Table 1, the specific surface area decreases in the course of the reaction compared to the fresh samples, in particular with respect to samples calcined at lower temperatures such as 100 and 200°C.

XPS results show that the amount of Au_2O_3 in used Au/Fe_2O_3-*T* (*T* = 100, 200, and 300) decreased noticeably compared to the fresh samples, indicating that the oxide gold was transformed into metallic Au during the reaction (Table 2). This is also demonstrated by TPR results. As shown in Fig. 6, the peak I (reduction peak of oxide gold to metallic gold) area in used Au/Fe_2O_3-*T* (*T* = 100–300) catalysts obviously increased compared to the fresh samples. For Au/Fe_2O_3-300 catalysts, peak I disappears completely. Park *et al.* [12, 27, 31] reported that the oxidized gold species were more active than metallic gold. Therefore, the reduction of Au oxide to metallic Au may be one of the reasons for the deactivation of Au/Fe_2O_3 catalysts. Furthermore, it can be seen from Fig. 6 that the T_{max} of Au oxide and iron oxide reduction peaks shift to a higher temperature, indicating that the interaction between Au species and Fe supports seem to weaken. It has to be noted that strong interaction between gold and supports and the formation of a well-defined interface between the two phases are critical for high activity [4–16]; therefore, these phenomena will influence the CO oxidation.

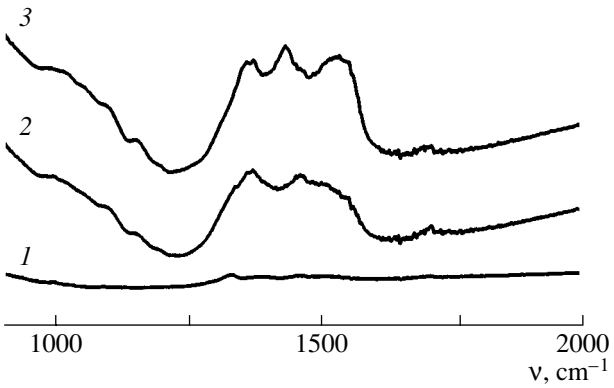

Fig. 8. *In situ* FTIR spectra of Au/Fe_2O_3 catalysts (*1*) before reaction, (*2*) after reaction for 24 h, and (*3*) 48 h. Sample as calcined at 300°C in air for 3 h, at the same temperature evacuated for 2 h, then cooled to 25°C, and introduced 26.7 kPa CO and 26.7 kPa O_2.

In situ FT-IR results for the CO + O_2 reaction at 25°C are shown in Fig. 8. It is clear that some strong bands in the 1000–1700 cm^{-1} region grow with the reaction time, indicating that carbonate-like species were formed on the surface of Au/Fe_2O_3 catalysts. Previous studies showed that the decomposition of carbonate-like species was a rate-determining step [3, 5, 9, 11, 21] and that the accumulation of carbonate may somewhat suppress the reaction of CO and O_2.

CONCLUSION

The catalytic stability of Au/Fe_2O_3 catalysts for CO oxidation has been investigated at ambient temperature and in the presence of water vapor. Several conclusions can be drawn: Gold supported on iron species exhibits excellent catalytic activity and stability for CO oxidation. The time-dependent deactivation is greatly affected by the precipitation method and calcination temperatures, because they affect the particle size of gold and iron, the specific surface area, the oxidation state of Au and iron crystallite, the interaction between gold and iron, etc. The particle size of gold is one of the main factors affecting the stability, and the lifetime of Au/Fe_2O_3 increases with a decrease in the gold particle size. During the reaction, the sintering of metallic gold, the reduction of gold oxide into metal, the weakening of interaction between Au and iron species, the reduction of SBET, and the formation of carbonate-like species on the surface of Au/Fe_2O_3 catalysts are observed, which may contribute to the deactivation of the Au/Fe_2O_3 catalysts.

ACKNOWLEDGMENT

This work was supported by the National Natural Science Foundation of China (grant no. 20073015), the Shan Xi Institute of Coal Chemistry, Chinese Academy of Sciences (1999), and the Key Project Foundation of the Ministry of Education, China (grant no. 1A301123).

REFERENCES

1. Murad, E. and Schwertmann, U., *Am. Mineral.*, 1980, vol. 65, p. 1044.
2. Funazaki, N., Hemmi, I.A., and Asano, S.Y., *et al.*, *Sens. Actuators, B*, 1993, vols. 13–14, p. 536.
3. Haruta, M., Tsubota, S., Kobatashi, T., *el al., J. Catal.*, 1993, vol. 144, p. 175.
4. Aderson, J.A., *J. Chem. Soc., Faraday Trans.*, 1992, vol. 88, p. 1201.
5. Kozolova, A.P., Sgiyama, S., and Kozlov, A.I., *et al.*, *J. Catal.*, 1998, vol. 176, p. 426.
6. Boccuzzi, F., Chiorino, A., Tsubota, S., and Haruta, M., *J. Phys. Chem.*, 1996, vol. 100, p. 3625.
7. Hoflund, G.B., Gardner, S.D., and Schryer, D.R., *Appl. Catal. B*, 1995, vol. 6, p. 117.
8. Hoflund, G.B., and Gardner, S.D., *Langmuir.*, 1995, vol. 11, p. 3431.
9. Bollinger, M.K., and Vannice, M.A., *Appl. Catal. B*, 1996, vol. 8, p. 414.
10. Grunwaldt, J.D., Kiener, C., Wogerbaoer, C., and Baiker, A., *J. Catal.*, 1999, vol. 181, p. 223.
11. Knell, A., Barnickel, P., Baiker. A., and Wokaun, A., *J. Catal.*, 1992, vol. 137, p. 306.
12. Park, E.D., and Lee, J.S., *J. Catal.*, 1999, vol. 186, p. 1.
13. Wanger, F.E., Galvagno, G., and Visco, A.M., *J. Chem. Soc. Faraday Trans.*, 1997, vol. 93, p. 3403.
14. Yuan, Y., Kozlova, A.P., Asakura, K., *et al., J. Catal.*, 1997, vol. 170, p. 191.
15. Okumura, M., Nakamura, S., Tsubota, S., *et al.*, *Catal. Lett.*, 1998, vol. 51, p. 53.
16. Yuan, Y., Asakura, K., Wan, H., Tsai, K., *et al.*, *Catal. Lett.*, 1996 vol. 42, p. 15.
17. Kozlova, A.P., Kozlov, A.I., Sugiyama, S., *et al.*, *J. Catal.*, 1999, vol. 181, p. 37.
18. Hutching, G.J., Siddiqui, M.R.H., Burrows, S., *et al.*, *J. Chem. Soc. Faraday Trans.*, 1997, vol. 93, p. 187.
19. Liu, Z.M. and Vannice, M.A., *Catal. Lett.*, 1997, vol. 43, p. 51.
20. Guillemot, D., Borrovkov, V., Kazansky, V.B., *et al.*, *J. Chem. Soc. Faraday Trans.*, 1997, vol. 93, p. 3587.
21. Bocuzzi F. and Chiorino, A., *J. Phys. Chem. B.*, 2000, vol. 104, p. 5414.
22. Ruth, K., Hayes, M., Burch, R., *et al.*, *Appl. Catal. A.*, 2000, vol. 24, p. L133.
23. Horváth, D., Toth, L., and Guczi, L., *Ctal. Lett.*, 2000, vol. 67, p. 117.
24. Guczi, L., and Horvath, D., *J. Phys. Chem. B.*, 2000, vol. 104, p. 3183.
25. Wang, G.Y., Zhang, W.X, Jiang, D.Z., *et al.*, *ACTA Chimica Sinica*, 2000, vol. 58, no. 12, p. 1557.
26. Wang, G.Y., Yu, J.Y., Lian, H.L., *et al.*, *Chem. J. Chin. Univ.*, 2000, vol. 5, p. 752.
27. Visco, A.M., Neri, F., Neri, G., *et al.*, *Phys.Chem. Chem. Phys.*, 1999, vol. 1, p. 2869.
28. Liu, H.C., Kozlov, A.I., Kozlova, A.P., *et al.*, *Phys. Chem. Chem. Phys.*, 1999, vol. 1, p. 2851.
29. Murad, E., *Phys. Chem. Mineral.*, 1996, vol. 65, p. 248.
30. Benz, M., Van der Kraan, A.M., and Prins, R., *Appl. Catal. A*, 1998, vol. 172, p. 149.
31. Finch, R.M., Hodge, N.A., Hunchings, G.J., *et al.*, *Phys. Chem. Chem. Phys.*, 1999, vol. 1, p. 485.
32. JCPDS International Center for Diffraction Date, *Powder Diffraction File*, Swarthmore, PA, 1991.
33. Ilieva, L.I., Andreeva, D.H., and Andreev, A.A., *Thermochim. Acta.*, 1997, vol. 292, p. 169.